ARTICLE

BIOTECHNOLOGY and BIOENGINEERING

A Kinetic-Based Approach to Understanding Heterologous Mevalonate Pathway Function in *E. Coli*

Lane J. Weaver,[1,2] Mirta M. L. Sousa,[1,5,6] George Wang,[1,3] Edward Baidoo,[1,3] Christopher J. Petzold,[1,3] Jay D. Keasling[1,2,3,4]

[1]Joint BioEnergy Institute, 5885 Hollis Avenue, Emeryville, California 94608; telephone: 510.495.2620; fax: 510.495.2630; e-mail: jdkeasling@lbl.gov

[2]UCB-UCSF Joint Graduate Group in Bioengineering, Berkeley, California 94720

[3]Physical Biosciences Division, Lawrence Berkeley National Laboratory, Berkeley, California 94720

[4]Department of Chemical & Biomolecular Engineering, University of California, Berkeley, California 94720

[5]Department of Cancer Research and Molecular Medicine, Faculty of Medicine, Norwegian University of Science and Technology (NTNU), Trondheim NO-7489, Norway

[6]The Proteomics and Metabolomics Core Facility (PROMEC) at NTNU, Trondheim, Norway

ABSTRACT: To aid in debugging efforts to increase yield, titer, and productivity of engineered metabolic pathways, computational models are increasingly needed to predict how changes in experimentally manipulable variables such as enzyme expression map to changes in pathway flux. Here, an ordinary differential equation model is developed for a heterologous mevalonate pathway in *E. coli* using kinetic parameters culled from literature and enzyme concentrations derived from Selective Reaction Monitoring Mass Spectrometry (SRM-MS). To identify parameters most important to further experimental investigation, a global sensitivity analysis was performed, which pointed to amorphadiene synthase activity as the main limiting factor for amorphadiene production. Furthermore, the model predicted that in this local enzyme expression regime, the overall pathway flux is insensitive to farnesyl pyrophosphate (FPP)-mediated inhibition of mevalonate kinase, not supporting a hypothesis that had previously been posited to be limiting amorphadiene production. To test these predictions experimentally, two strains were constructed: (1) a strain containing a homologous mevalonate kinase with weaker feedback inhibition, and (2) a strain with greater amorphadiene synthase expression. The experimental results validate the qualitative model hypotheses and accurately match the predicted productivities for the two strains, particularly when an in vivo-derived k_{cat} for amorphadiene synthase was substituted for the literature value. These results demonstrate the utility of using kinetic representations of engineered metabolic pathways parameterized with experimentally derived protein concentrations and enzyme kinetic constants to predict productivities and test hypotheses about engineering strategies.

Biotechnol. Bioeng. 2015;112: 111–119.

KEYWORDS: kinetic modeling; proteomics; metabolic engineering; isoprenoids

Correspondence: J.D. Keasling

Received 14 April 2014; Revision received 17 June 2014; Accepted 25 June 2014
Accepted manuscript online 1 July 2014;
Article first published online 19 August 2014 in Wiley Online Library (http://onlinelibrary.wiley.com/doi/10.1002/bit.25323/abstract).
DOI 10.1002/bit.25323

Introduction

Metabolic engineers have made considerable progress in producing biologically derived chemicals over the last 30 years, due in part to increases in experimental productivity—notably improvements in DNA synthesis and assembly technologies—which enable faster experimental cycle time.

Modeling efforts have been developed in parallel in an attempt to increase the experimental "hit rate", guiding the researcher toward experiments more likely to yield the desired result. These efforts have predominately focused on stoichiometric, flux-based models, which can provide a wealth of information about distribution of carbon in metabolism. However, these models are typically not predictive unless optimization criteria are applied via an objective function (e.g., growth maximization)—an assumption that may not be accurate for engineered strains that have not been subjected to countervailing evolutionary pressures.

Furthermore, flux-based models do not explicitly treat enzyme concentration as a (continuous) variable, creating a disconnect with experiment, as expression levels are one of the main ways used to manipulate engineered pathways.

Kinetic models, on the other hand, can provide a great deal of information about a pathway, supplying the time-evolution of substrate, intermediate, and product concentrations. An experimenter can alter enzyme production levels in silico and directly observe their effect on pathway flux. However, kinetic models are typically difficult to employ due to the lack of parameters (e.g., rate constants, enzyme concentrations) available for most systems. Additionally, even in situations where in vitro kinetic constants have been characterized, the fidelity of these constants to in vivo environments remains an open question (García-Contreras et al., 2012; Laue and Demeler, 2011; van Eunen et al., 2010).

One method of addressing these issues computationally is to intentionally allow the model parameters to vary, randomly sampling them about some prescribed initial or mean value, and then solving the system equations for each generated parameter set. This model ensemble can then be examined statistically to identify the parameters with the greatest impact on the relevant output. While this global sensitivity analysis provides a valuable starting point for more targeted investigations, its predictive ability is by its nature somewhat imprecise. In general, the more parameters that can be measured with small error, the more prescriptive the model will become.

Here, we build an Ordinary Differential Equation (ODE) model of a heterologous mevalonate pathway in *E. coli*, which converts mevalonate into farnesyl pyrophosphate (FPP) that can then by cyclized by amorphadiene synthase (ADS) to produce amorphadiene, providing a readout of pathway activity (Fig. 1). We address the parameterization of this model in two ways: (1) by measuring absolute protein concentrations via Selective Reaction Monitoring Mass Spectrometry (SRM-MS) using a synthetic protein standard curve, and (2) by using steady-state enzyme kinetic parameters borrowed from literature. Using global sensitivity analysis, we identify the most important factor for production in the enzyme expression regime of a base strain—the concentration of amorphadiene synthase (ADS). Additionally, we observe from direct inspection of the model that amorphadiene production is insensitive to changes in the strength of FPP-mediated feedback inhibition of mevalonate kinase, which had previously been suspected to be limiting flux through the pathway.

To test these model-generated hypotheses, we constructed a strain with higher ADS expression (which would be predicted to yield higher productivity) and a strain encoding a mevalonate kinase with a weaker $K_{i,MK\text{-}FPP}$ (which we predict would not affect amorphadiene productivity). Using mevalonate as a substrate, we disconnect the pathway from central carbon metabolism, allowing us to examine amorphadiene productivity largely independently from complicating factors of cell physiology. When we compare absolute amorphadiene productivities between model and experiment in these systems, we find good agreement.

Materials and Methods

Growth & Media

Plasmids were freshly transformed into *E. coli* DH1 for each experiment. Colonies were picked the next day and used to inoculate overnight cultures in LB medium. The following day, 200 μL overnight culture was diluted in 50 mL LB medium supplemented with 50 mg/L carbenicillin and 0.5% (w/v) glucose and induced with 1 mM IPTG when the optical density at a wavelength of 600 nm (OD_{600}) reached 0.6. Two hours later, 2 mL of 1 M mevalonate was added (40 mM final concentration) and 20% (v/v) dodecane was overlayed to capture the volatile sesquiterpene. Time points were sampled every two hours as follows: 0.25 mL of culture was used to measure OD_{600}, and 1.5 mL of culture was harvested through centrifugation (8000 × g, 8 min, 4°C) for various analyses: for extracellular metabolites, 250 μL of the supernatant was added to 250 μL ice cold methanol, filtered through a 3 kDa membrane, and stored at −20°C until LC-MS analysis. The remaining supernatant was discarded and the resultant pellet

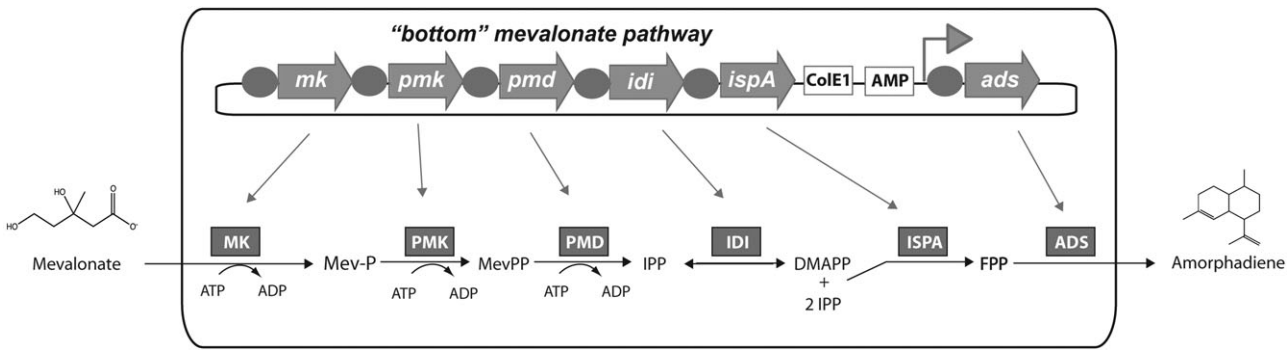

Figure 1. Overview of a heterologous bottom portion of the mevalonate pathway in *E. coli*. All enzymes are expressed polycistronically from a pTrc promoter on a ColE1 plasmid. Mevalonate is fed exogenously and is converted through the set of intracellular reactions to amorphadiene, which freely crosses the cell membrane and can be recovered extracellularly.

was resuspended in 300 μL ice-cold methanol, and stored at −20°C until intracellular metabolite and protein analysis.

Targeted Proteomics

240 μL of water and 150μL of chloroform were added to the 300 μL methanol pellet from the previous section, vortexed, and centrifuged (14000 × g, 10 min, 4°C) to create 3 phases: 540 mL of aqueous (methanol/water) on top, a *protein interface*, and 150 μL chloroform on the bottom. The top layer was harvested and kept at −20°C for metabolite analysis, while the remaining protein and chloroform mixture was resuspended in 300μL methanol, vortexed, and centrifuged (14,000 × g, 2 min, RT). The supernatant was discarded and the pellet was dried in a speed-vac for 45 min.

The dried protein pellet was resuspended in 10 μL methanol and 90 μL of 100 mM ammonium bicarbonate. This solution was vortexed and the concentration measured by DC Protein Assay (BioRad). Protein samples were normalized to 1 mg/mL in 100 mM ammonium bicarbonate and 10% (v/v) methanol, followed by cysteine reduction with 5 mM TCEP and subsequent alkylation with 4 mM iodoacetic acid. The samples were digested with 0.02 mg/mL trypsin for 16 h at 37°C, and then frozen until analysis.

Proteomic Selected Reaction Monitoring (SRM) was performed on a 6460QQQ mass spectrometer (Agilent Technologies) interfaced to a 1260 liquid chromatography system. Peptides (5 μg) were injected onto an Ascentis Peptide Express C-18 column (2.1 mm × 50 mm)(Sigma) via an Agilent G1377A autosampler and separated using a 22-min method as previously described (Batth et al., 2012). SRM method development and data analysis were performed by using the Skyline software version 2.0 (MacLean et al., 2010).

Modeling Studies

An ordinary differential equation model was built in Mathematica (Wolfram Research) using the kinetic parameters given in Supplementary Table II and enzyme concentrations determined by quantitative proteomic analysis (Supplementary Table III); the latter were found to be approximately constant throughout the course of the experiment post-mevalonate addition (data not shown). Initial metabolite concentrations were set to 100 nM based on two factors: 1) experiments performed on native DH1 cells were unable to detect any mevalonate pathway intermediates, suggesting they fall under the limit of detection and are thus very low abundance species, and 2) manual testing of the model demonstrated it to be insensitive to at least 10-fold changes in concentrations of all initial intermediate species. The mevalonate concentration was set at (constant) 5 mM, the average of experimental LC-MS data for the intracellular concentration over the time period of the model, which was 8 h. Since, apparent K_m's were reported for all reactions utilizing ATP (i.e., K_m's were not determined as a function of [ATP]), the ATP concentration was assumed to be constant and saturating for the entire simulation time.

The method of Carothers et al. (Carothers et al., 2011) was used for the global sensitivity analysis. Briefly, a custom perl script was written to generate random parameter sets sampled from a uniform distribution ranging 10-fold above and 10-fold below each of the Michaelis–Menten constants and enzyme concentrations. A set of 10,000 of these models was simulated on a server cluster using Dizzy, a Java-based chemical kinetics simulation program (Ramsey et al., 2005), generating a 10,000 product outputs. The sensitivity to each parameter was analyzed with partial rank correlation coefficients using the R statistical programming language.

Measurement of Pathway Intermediates and Amorphadiene

Liquid Chromatography-Mass Spectrometry

Chemical standards were made up to 200 μM, as the stock solution, in methanol-water (50:50, v/v). The separation of the mevalonate pathway intermediates was conducted on a ZIC-pHILIC column (150 mm length, 4.6-mm internal diameter, and 5-μm particle size; from Merck SeQuant) using an Agilent Technologies 1200 Series HPLC system (Agilent Technologies, CA, USA) with 3 μL injection volume. The temperature of the sample tray was maintained at 4°C using an Agilent FC/ALS Thermostat. The column compartment was set to 40°C. The mobile phase was composed of (A) 10 mM ammonium carbonate and 0.5% ammonium hydroxide in acetonitrile-water (2:8, v/v) and (B) 10 mM ammonium carbonate and 0.5% ammonium hydroxide in acetonitrile-water (8:2, v/v). Mevalonate pathway intermediates were eluted isocratically with a mobile phase composition of 33% mobile phase A and 67% of mobile phase B. A flow rate of 0.45 mL/min was used throughout. The HPLC system was coupled to an Agilent LC/MSD SL single quadrupole mass spectrometer (LC-MS) by a 1/3 post-column split. The LC-MS system was controlled by the Chemstation (Agilent Technologies, CA, USA) software package. Contact between both instrument set-ups was established by a LAN card in order to trigger the MS into operation upon the initiation of a run cycle from Chemstation. ESI-MS was conducted in the negative ion mode, and a capillary voltage of 3500 V was utilized. MS experiments were carried out in the selected ion monitoring mode, with a dwell time of 200 ms, for the detection of $[M - H]^-$ ions. The instrument was tuned for a range of 50–2000 m/z. The LC/MSD SL was calibrated externally by the Agilent ES tune mix (Agilent Technologies, Santa Clara, CA, USA). Data acquisition and processing were performed by Agilent Chemstation. Mevalonate from *E. coli* extracts was quantified via seven-point calibration curves ranging from 625 nM to 200 μM. The R^2 coefficients for the calibration curves were $\geq$0.99.

Gas Chromatography-Mass Spectrometry

Amorphadiene production was measured by GC-MS by diluting 10 μL of the dodecane overlay into 990 μL ethyl

acetate spiked with a caryophyllene internal standard. 1 μL of the sample was injected into an Agilent 6890 series gas chromatograph (GC) equipped with an Agilent 5973 mass selective (MS) detector and a CycloSil-B (chiral) capillary column (30 m × 250 μm× 0.25 μm thickness; Agilent). The GC oven temperature program was as follows: 100°C for 45 s, a ramp of 35°C/min–200°C, a ramp of 100°C/min–250°C, and a hold at 250°C for 1 min. The MS was operated in selected ion monitoring (SIM) mode monitoring for the molecular ion at 204 m/z and fragment ion at 189 m/z.

Amorphadiene concentrations were quantified by comparing caryophyllene-normalized sample peak areas to those of an authentic amorphadiene standard curve. Normalized rates were obtained by converting to the apparent intercellular concentration using the conversion factors in Supplementary Equations 1 and 2, subtracting the concentrations at 2 and 8 h, and then dividing by the time.

Results

Targeted Proteomic Analysis Provides Absolute Enzyme Concentrations for Model Construction

Protein concentrations derived from proteomics measurements are typically reported in relative units, which are not appropriate for use in modeling studies. To obtain absolute protein concentrations, peak areas measured on the mass spectrometer need to be compared to the areas of a standard of known concentration. We constructed a synthetic polypeptide (Mev2.0) containing a pre-validated set of peptide fragments from each of the mevalonate pathway enzymes (as listed in Supplementary Table I) to use as a standard. By measuring the concentration of the Mev2.0, typsinizing to release each peptide, and individually quantitating on the mass spectrometer, we were able to derive calibration curves for each of the mevalonate pathway enzymes. Of the peptides measured, 18 have R^2 values greater than 0.97 based on a linear dilution series. To then obtain starting values of absolute enzyme concentrations for model construction, we transformed pMBIS3 into DH1 cells to obtain a base strain, mbis3, and used these calibration curves to calculate the expression levels of each mevalonate pathway enzymes. These values were then converted to cellular concentrations via Supplementary Equation 2. The resulting absolute, cellular concentrations are shown in Figure 2.

Global Sensitivity Analysis Identifies Amorphadiene Synthase Expression and Activity as Most Important Parameters for Production

To determine which reactions were most important to overall pathway flux and thus good candidates for more targeted examination, we performed a global sensitivity analysis, simulating the pathway thousands of times with randomly sampled parameters. Literature values were used as starting points for the Michaelis–Menten parameters, while the absolute, cellular concentrations derived from the targeted proteomic analysis of base strain mbis3 were used as starting values for enzyme concentrations. We mapped changes in these parameters to the rate of amorphadiene production using a partial rank correlation coefficient, which provides a sensitivity measure for monotonic, nonlinear relationships between input and output parameters when little or no correlation exists between the inputs (Marino et al., 2009).

As shown in Figure 3, amorphadiene production is most strongly correlated with both the concentration and K_{catADS} of ADS, suggesting that the last enzyme in the pathway is a good candidate for further investigation. A secondary point of control appears to lie with IspA.

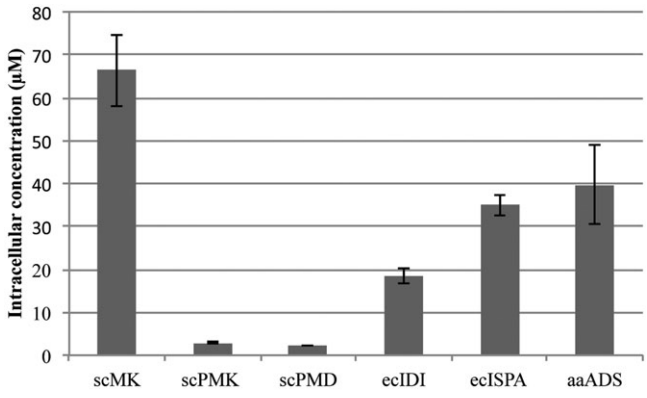

Figure 2. Absolute, intercellular concentrations of enzymes for a base strain (mbis3) of the bottom mevalonate pathway: scMK, *S. cerevisiae* mevalonate kinase; scPMK, *S. cerevisiae* phosphomevalonate kinase; scPMD, *S. cevervisiae* phosphomevalonate decarboxylase; ecIDI, *E. coli* IPP isomerase; ecISPA, *E. coli* FPP synthase; aaADS, *A. annua* amorphadiene synthase. Error bars represent standard deviations about the mean for three biological replicates.

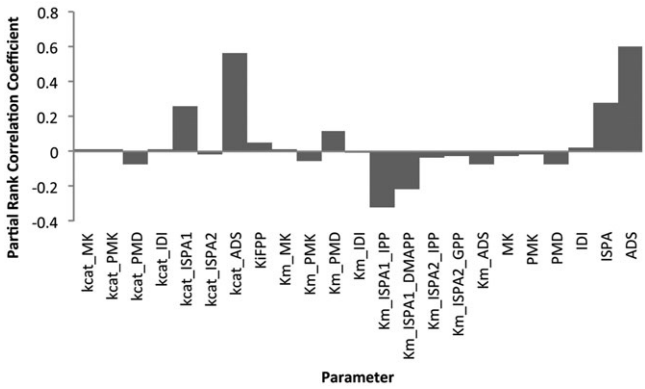

Figure 3. Global sensitivity analysis of mevalonate pathway parameters given in Supplementary Tables II and III, as measured by the partial rank correlation coefficient for the rate of amorphadiene production.

FPP Measurement Enables More Accurate Determination of ADS K_{cat}

Given that K_{catADS} was identified to be one of the most important parameters for the prediction of amorphadiene productivity, we sought to derive an in vivo K_{cat} that could be compared with the in vitro literature value, and, if different, used for subsequent simulations.

First, to determine if FPP levels were in a saturating regime in which we could extract the V_{max} of amorphadiene synthase, we fed mevalonate to mbis3, measuring FPP levels via LC-MS and converting into cellular concentrations using the correction factors given in Supplementary Equation 1. As observed in Figure 4, the FPP levels for the MBIS3 strain are reliably saturating ADS ($K_M = 3.3\ \mu M$) throughout the timecourse of the experiment (8 h), suggesting that the measured, normalized amorphadiene productivities for these strains were in fact $V_{max,ADS}$.

Thus, using the concentrations of ADS as determined by SRM-MS, the normalized amorphadiene productivity calculated using GC-MS data, and the following equation

$$k_{cat} = \frac{V_{max}}{[ADS]}$$

we estimated $k_{cat\ ADS,\ in\ vivo}$ to be $0.022 \pm 0.008\ s^{-1}$. This number is approximately 3-fold higher than the value derived by in vitro studies ($0.0068\ s^{-1}$) (Picaud et al., 2005).

Attenuating Feedback Inhibition as an Engineering Strategy

Next, we sought to test hypotheses about mevalonate pathway engineering strategies with the model. The first hypothesis was borne out of structural and functional data showing that mevalonate kinase (MK), the first enzyme in the bottom part of the pathway, is inhibited by FPP, the final intermediate in the pathway (Miziorko, 2011). It thus suggested that this reaction might be a suitable target for pathway engineering efforts, perhaps by replacing the *S. cerevisiae* MK with a homologous version with weaker feedback inhibition.

To test the dependence of amorphadiene productivity on the $K_{i,MK\text{-}FPP}$, we simulated the pathway several times, with values of the inhibition constant 3 orders of magnitude higher and lower than the nominal value ($K_i = 1.9\ \mu M$). The rate of amorphadiene production changed by no more than 3% in this six order-of-magnitude range, suggesting that the pathway flux was insensitive to changes in this parameter.

To experimentally test the fidelity of this prediction, we transformed pMBIS3-saMK into DH1 to obtain strain saMK, which contained a homologous mevalonate kinase from *S. aureus* with a 24-fold weaker $K_{i,MK\text{-}FPP}$ (Voynova et al., 2003). Enzyme expression levels were remeasured and entered into the model to determine a predicted amorphadiene productivity, which was then compared against the experimental amorphadiene productivity calculated via GC-MS data, as done previously for the base strain, mbis3. As Figure 5 shows, the predicted rate of amorphadiene production closely matches its experimental value and is also within the error of the base strain, supporting the notion that amorphadiene production was not sensitive to mevalonate kinase inhibition in this particular context, as the model predicted, thus validating the assertion that mevalonate kinase was not a good target for engineering efforts.

Increasing ADS as an Engineering Strategy

Since, the global sensitivity analysis pointed to the primary importance of ADS concentrations to amorphadiene production, we directly tested the effect of increasing ADS expression levels on productivity using the model. As expected, amorphadiene productivity increased with

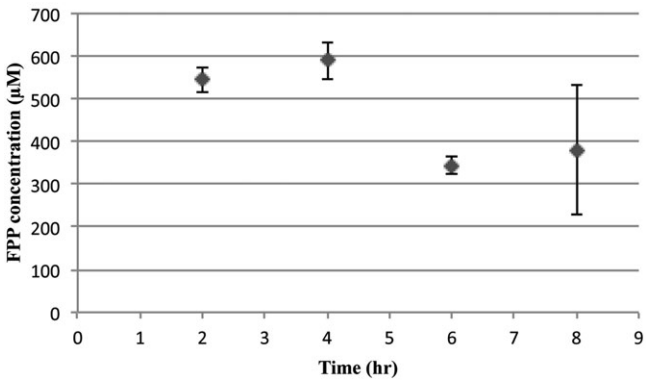

Figure 4. Intercellular concentration of FPP in base strain, mbis3, over experimental time-course. Error bars represent standard deviations about the mean for three biological replicates.

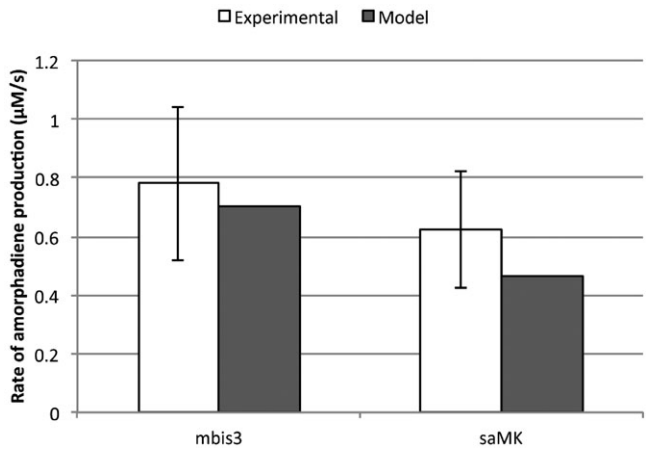

Figure 5. Experimental rate of amorphadiene production compared to model-predicted rate for the saMK strain. Error bars represent standard deviations about the mean for three biological replicates.

Table I. List of strains and plasmids.

Plasmid name	Description	Reference
pMBIS3	ColE1, pTrc-aaADS-scMK-scPMK-scPMD-ecIDI-ecISPA, AmpR	Nowroozi et al., (2014)
pMBIS3-saMK	ColE1, pTrc-aaADS-saMK-scPMK-scPMD-ecIDI-ecISPA, AmpR	This work
pMBIS3-10kADS	ColE1, pTrc-10kRBS-aaADS-scMK-scPMK-scPMD-ecIDI-ecISPA, AmpR	This work
pET-Mev2.0	ColE1, pT7-Mev2.0-His	This work
Strain name	**Description**	**Reference**
DH1	*Escherichia coli F- supE44 hsdR17 recA1 gyrA96 relA1 endA1 thi-1 λ-*	Hanahan et al. (1983)
DH10B	*F- mcrAΔ(mrr-hsdRMS-mcrBC) φ80lacZΔM15 ΔlacX74 recA1 endA1 araD139 Δ(ara, leu) 7697 galUgalK λ- rpsLnupG*	Invitrogen

increasing ADS expression, although in an asymptotic fashion. To understand the cause of this non-linear effect, we also plotted the concentration of FPP at increasing ADS expression levels. As ADS is overexpressed in silico, the concentration of FPP becomes comparable to the K_m of ADS, at which point the rate of amorphadiene production levels off (Fig. 6). In this regime, precursor supply is unable to keep pace with the flux through ADS.

To verify the impact of ADS on amorphadiene production, we constructed another strain with a computationally designed, stronger ribosome binding site in front of ADS (10kADS), by transforming DH1 with pMBIS3-10kADS. This strain increased the expression of ADS ~10-fold, as measured by SRM-MS. Using the new concentrations of pathway enzymes determined as before by SRM-MS, we re-simulated the pathway and obtained a new value for the predicted amorphadiene production. Again, we find good congruence between the predicted and experimental productivities (Fig. 7).

Elucidating the Role of Feedback in the Two Strains

While the use of mevalonate kinase homologue with weaker feedback inhibition was shown to be an ineffective strategy to increase amorphadiene production, the root of this effect was unclear. To clarify, we again turned to the model. Examining the rate of mevalonate–phosphate synthesis for the base strain and for the two modified strains, we observe that saMK, with weaker feedback inhibition, has a greater rate of mevalonate–phosphate synthesis than mbis3, as expected (Fig. 8A). However, perhaps surprisingly, the 10kADS exhibits the highest rate overall of mevalonate–phosphate synthesis of the three strains. The cause of the increased mevalonate–phosphate synthesis becomes evident when the FPP levels for each strain are plotted as well (Fig. 8B). The 10kADS strain, by virtue of having the lowest FPP levels, has the lowest inhibitory effect on the upstream part of the pathway. This is supported by experimental metabolite levels in Figure 8C, assuming that the faster rate of mevalonate phosphate synthesis results in higher accumulation of that metabolite in the three strains.

However, it is important to distinguish the source of the improvement in the rate of amorphadiene production from the increased rate of upstream precursors—while the 10kADS strain has greater flux through the upstream portion of the pathway, FPP levels are still saturating ADS. Thus, it is the increased expression of ADS that is driving the increase in the rate of amorphadiene synthesis, not the increased precursor supply. This notion is further supported by the fact that computationally titrating $K_{i,MK\text{-}FPP}$ in either direction about its nominal value in the 10kADS strain

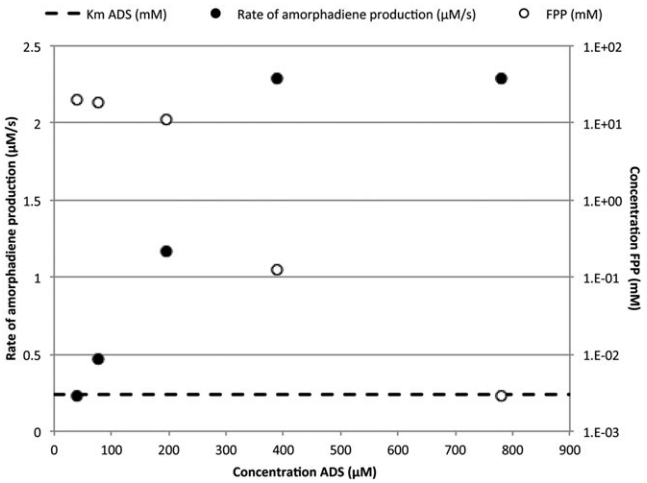

Figure 6. Simulated dependence of amorphadiene production and FPP concentration on ADS expression.

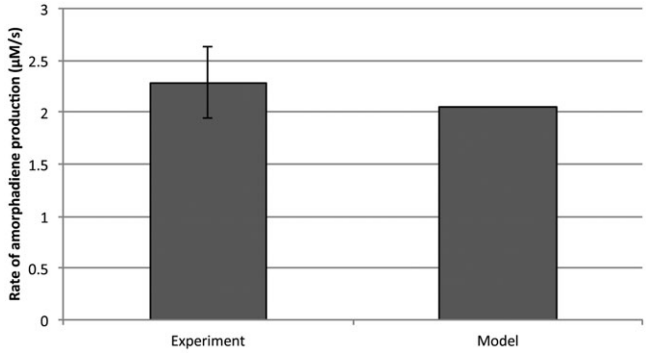

Figure 7. Experimental rate of amorphadiene production compared to model-predicted rate for the 10kADS strain. Error bars represent standard deviations about the mean for three biological replicates.

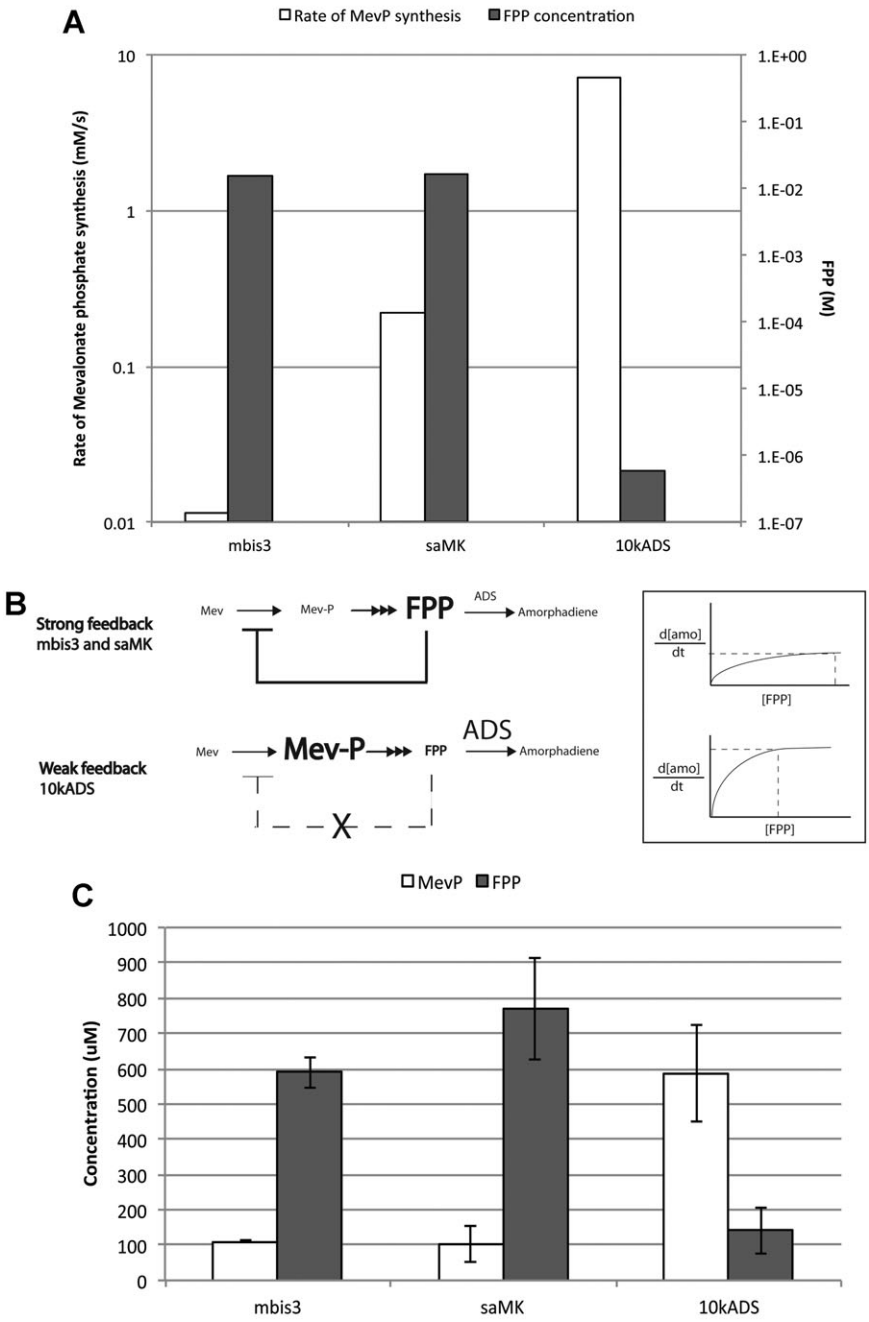

Figure 8. A: Simulated effect of feedback inhibition on mevalonate phosphate synthesis. The rate of mevalonate phosphate synthesis (white bars) increases if (1) inhibition is attenuated by using a different mevalonate kinase, as in saMK, or (2) if FPP levels drop below the K_i, as in the 10kADS strain. B: In the left panel, graphical representation of feedback inhibition in high feedback (mbis3, saMK) and low feedback (10kADS) strains. The right panel illustrates the relative FPP concentrations and ADS velocities for these high feedback and low feedback scenarios. C: Experimental concentrations of mevalonate phosphate (white bars) and FPP (black bars) for the mbis3, saMK, and 10kADS strains. Error bars represent standard deviations about the mean for three biological replicates.

causes no change in the rate of amorphadiene production (data not shown).

Discussion

Despite many years of engineering efforts, there is still no definitive way to predict how expressing a particular enzyme at a certain level will impact production, which can largely be attributed to the lack of availability of kinetic pathway models.

Here we built a base ODE model of the mevalonate pathway, using kinetic constants taken from literature and enzyme concentrations derived from SRM-MS experiments. By using mevalonate as the substrate for the pathway, we

effectively decoupled pathway function from central carbon metabolism, simplifying the set of necessary equations and elimination and any transcriptional or translation regulatory interactions that may have affected pathway dynamics. This allowed us to study the kinetics of the mevalonate pathway independently of these confounding factors, which led to good agreements between predicted and experimental amorphadiene productivities when enzyme levels and identities were manipulated.

We used the model to examine hypotheses about engineering strategies for increasing amorphadiene production. First, we demonstrated that the inhibition of mevalonate kinase does not have a large effect on amorphadiene production. We verified this experimentally by replacing the *S. cerevisiae* mevalonate kinase with a *S. aureus* version that had weaker feedback inhibition, showing that the predicted amorphadiene productivity closely matched that of the experiment.

Based on the results of a global sensitivity analysis, we then tried a different engineering strategy of increasing ADS expression. Again, after inserting the experimental concentrations of pathway enzymes, we were able to obtain excellent agreement between predicted and experimental productivities. We expect that further refinement of the model, including the addition of reversibility and product inhibition terms, will in the future enable many more hypotheses to be first screened in silico, so that smaller number of better-guided experiments can be performed in the downstream engineering process.

With these results, we also showed that in vitro constants can be used to parameterize in vivo models, but may they have small errors associated with them, as was the case for the turnover number of ADS. This supports the use of dynamic models that explicitly consider parameter uncertainties, providing probabilistic distributions of outcomes, rather than definitive ones (Breitling et al., 2013).

This work additionally highlights the importance of terpene synthase engineering efforts to increasing mevalonate pathway flux, as an increase in ADS expression to ~600uM (~20% of cellular protein assuming 3 mM total) in the 10kADS strain still left the enzyme saturated with FPP substrate. The wide kinetic mismatch between terpene synthases and the rest of the mevalonate pathway enzymes suggests that this issue will become even more prominent if the pathway is genomically integrated (with a corresponding decrease in copy number), as would be likely for more industrial applications. Directed evolution may provide recourse to the inability to highly overexpress the enzyme from a genomic context. However, while a handful of examples of terpene synthase directed evolution exist, most have improved thermostability (Lauchli et al., 2013) or altered product selectivity (Yoshikuni et al., 2006); examples of improving activity are more rare (Leonard et al., 2010). This could be due to physiochemical constraints do not allow these reactions to proceed at a higher rate, but another explanation is that faster terpene synthases have not been selected for since enzymes of secondary metabolism typically do not experience the same magnitude of flux as central carbon metabolism, due to the fan-out effect of the latter (Bar-Even et al., 2011).

Looking forward to more sophisticated models, it is clear that the interactions between a pathway and the rest of the cell cannot be ignored. These effects are particularly important in the mevalonate pathway, where intermediate accumulation has been shown to affect both cell growth and glucose utilization. Also, the predicted high rate of mevalonate phosphate synthesis suggests that there may be additional production inhibition that was unaccounted for in this model, perhaps with mevalonate phosphate itself and/or downstream diphosphate intermediates. Thus, while this study demonstrated that the proximate kinetics of a pathway can successfully predict the rate of amorphadiene product formation, future models will likely need to incorporate additional considerations (e.g., inhibition of glycolytic enzymes by diphosphate intermediates, growth, reversible enzyme kinetics and product inhibition) to accurately predict both titers and steady-state intermediate concentrations using glucose as a carbon source.

We greatly appreciate the help of James Carothers with scripts for the global sensitivity analysis. This work was supported by the Synthetic Biology Engineering Research Center (SynBERC), which is funded by the National Science Foundation (grant number EEC-0540879), and by the DOE Joint BioEnergy Institute, which is funded by the U.S. Department of Energy, Office of Science, Office of Biological and Environmental Research through contract DE-AC02-05CH11231.

References

Bar-Even A, Noor E, Savir Y, Liebermeister W, Davidi D, Tawfik DS, Milo R. 2011. The moderately efficient enzyme: evolutionary and physicochemical trends shaping enzyme parameters. Biochemistry 50:4402–4410.

Batth TS, Keasling JD, Petzold CJ. 2012. Targeted Proteomics for Metabolic Pathway Optimization, In: Totowa, NJ: Humana Press. pp. 237–249.

Breitling R, Achcar F, Takano E. 2013. Modeling Challenges in the Synthetic Biology of Secondary Metabolism. ACS Synth Biol 2:373–378.

Carothers JM, Goler JA, Juminaga D, Keasling JD. 2011. Model-Driven Engineering of RNA Devices to Quantitatively Program Gene Expression. Science 334:1716–1719.

García-Contreras R, Vos P, Westerhoff HV, Boogerd FC. 2012. Why in vivomay not equal in vitro- new effectors revealed by measurement of enzymatic activities under the same in vivo-like assay conditions. FEBS J 279:4145–4159.

Hanahan D. 1983. Studies on Transformation of Escherichia coli with Plasmids. J Mol Biol 166:557–580.

Lauchli R, Raben K, Kalbarcyk K, Tata A, Heel T, Kitto R, Arnold FH. 2013. High-Throughput Screening for Terpene-Synthase-Cyclization Activity and Directed Evolution of a Terpene Synthase. Angew Chem 125:5681–5684.

Laue T, Demeler B. 2011. A postreductionist framework for protein biochemistry. Nat Chem Biol 7:331–334.

Leonard E, Ajikumar PK, Thayer K, Xiao W, Mo J, Tidor B, Stephanopoulos G, Prather KJ. 2010. Combining metabolic and protein engineering of a terpenoid biosynthetic pathway for overproduction and selectivity control. PNAS 107:13654–13659.

MacLean B., et al., 2010. Skyline: an open source document editor for creating and analyzing targeted proteomics experiments. Bioinformatics 26:966–968.

Marino S, Hogue IB, Ray CJ, Kirschner DE. 2009. A Methodology For Performing Global Uncertainty And Sensitivity Analysis In Systems Biology. J Theor Biol 254:178–196.

Miziorko HM. 2011. Enzymes of the mevalonate pathway of isoprenoids biosynthesis. Arch Biochem Biophys 505:131–143.
Nowroozi FF., et al. 2014. Metabolic pathway optimization using ribosome binding site variants and combinatorial gene assembly. Appl Micro Biotech 98:1567–1581.
Picaud S, Olofsson L, Brodelius M, Brodelius PE. 2005. Expression, purification, and characterization of recombinant amorpha-4,11-diene synthase from Artemisia annua L. Arch Biochem Biophys 436:215–226.
Ramsey S, Orrell D, Bolouri H. 2005. Dizzy: stochastic simulation of large-scale genetic regulatory networks. J Bioinform Comput Biol 3:415–436.
van Eunen K, Bouwman J, Daran-Lapujade P, Postmus J, Canelas AB, Mensonides FIC, Orij R, Tuzun I, van den Brink J, Smits GJ, Van Gulik WM, Brul S, Heijnen JJ, de Winde JH, de Mattos MJT, Kettner C, Nielsen J, Westerhoff HV, Bakker BM. 2010. Measuring enzyme activities under standardized in vivo-like conditions for systems biology - van Eunen -2010 - FEBS Journal - Wiley Online Library. FEBS J 277:749–760.
Voynova NE, Rios SE, Miziorko HM. 2003. Staphylococcus aureus Mevalonate Kinase: Isolation and Characterization of an Enzyme of the Isoprenoid Biosynthetic Pathway. J Bacteriol 186:61–67.
Yoshikuni Y, Martin VJJ, Ferrin TE, Keasling JD. 2006. Engineering Cotton (+)-δ-Cadinene Synthase to an Altered Function: Germacrene D-4-ol Synthase. Chem Biol 13:91–98.

Supporting Information

Additional Supporting Information may be found in the online version of this article at the publisher's web-site.